# Damage Due to Spot Cavitation on Hemispherical Cylindrical Body (Comparison between Isolated Cavity and Parallel Cavities)

**Seiji Shimizu, Akihiro Ihara, Motoo Okada, and Motoyasu Sakurai**
Hiroshima Institute of Technology, 2-1-1, Miyake, Saeki-ku, Hiroshima 731-5193, JAPAN

## Abstract

When the Reynolds number is larger than the critical value or laminar separation is eliminated by a trip installed on a hemispherical cylindrical body, attached spot cavitation is observed occasionally. It occurs at fixed place in the vicinity of the minimum mean pressure and grows into a triangular wedge. In the present investigation, isolated and parallel spot cavitation is artificially generated on the hemispherical body and the behavior of the cavitation is observed by instantaneous photographs. The frequency of damaging blows in the range of the flow speed of 25 to 50 m/s is obtained by counting the number of pits on an aluminum specimen. When spot cavitation occurs adjacently, the cavities become rather stable. The pitting rate at the maximum damage zone by the parallel spot cavitation is much smaller than that by the isolated spot cavitation. The total pitting rats at the maximum damage zone by the isolated and parallel spot cavitation vary roughly 5th power of the flow speed for the both cases.

## 1 Introduction

Since cavitation damage is strongly dependent on type of cavitation, the relationship between the type of cavitation and the intensity of cavitation damage must be clarified to predict cavitation damage quantitatively. Various types of cavitation on a hemispherical cylindrical body have been studied by many investigators (Hall & Carroll 1981, Pan, Yang & Hsu 1981, Huang 1986). When the Reynolds number is smaller than the critical value, the hemispherical body exhibits transition downstream from laminar separation. In this situation, sheet cavitation is observed around the body. Murai et al. 1997 studied the velocity dependence of damage by sheet cavitation around a hemispherical cylindrical body. When the Reynolds number increases to and above the critical value or the laminar separation is eliminated by a trip installed on the body, sheet cavitation is swept away but attached spot cavitation is observed occasionally. It occurs at fixed places in the vicinity of the minimum mean pressure and grows into a triangular wedge. It is considered that spot cavitation is due to isolated local roughness on the surface (Pan, Yang & Hsu 1981). The present authors investigated cavitation damage by isolated spot cavitation around a hemispherical cylindrical body (Shimizu, Tsurusaki, Hara & Nakagawa 1998).

In the present report, experimental studies are conducted to clarify the damage due to parallel spot cavitation on a hemispherical cylindrical body. The behavior of artificially generated parallel spot cavitation is observed by using instantaneous photographs. The frequencies of damaging blows in the range of the flow speed of 25 to 50 m/s are obtained by counting the number of damage pits on an aluminum specimen. The distributions of the damage pits and the variations of the pitting rate with the flow speed by the parallel spot cavitation are compared with those by the isolated spot cavitation.

## 2 Experimental apparatus and method

The experiments are conducted in a closed circuit water tunnel of the Hiroshima Institute of Technology. The diameter and the length of the working section are 62.5 and 1075 mm, respectively. The maximum velocity in the working section is 50 m/s. Water temperature in the tunnel is maintained 23±2 degrees centigrade by using cooling units in reservoir tanks. For further details of the tunnel, the reader may refer to Murai et al. 1997.

A hemispherical nosed cylindrical body used in the experiments, consisting of a hemispherical head, a test specimen, and a cylindrical body is shown in Figure 1. The diameter of the cylindrical body is 25 mm. The joints of each part are carefully finished not to affect the aspect of cavitation. The cylindrical test specimens made of commercially available pure aluminum (JIS A1050) are used for erosion tests. Chemical composition of the specimen is shown in Table 1. The hemispherical head and the cylindrical body are made of stainless steel (JIS SUS304). The surface roughness of the specimen is less than $R_{max}$=1.2 μm.

Table 1 Chemical composition of specimen

| | Si | Fe | Cu | Mg | Ti | Al |
|---|---|---|---|---|---|---|
| A1050 | 0.07 | 0.14 | 0.01 | 0.01 | 0.01 | 99.76 |

Figure 2 shows the hemispherical head used in the erosion tests. In the present investigation, spot cavitation is artificially generated from a hollow with a diameter of 0.2 mm downstream from a boundary-layer trip installed on the hemispherical heads. The location of the trip is 30 degrees from the stagnation point and the height of the trip is 0.15 mm (Shimizu, Tsurusaki, Hara & Nakagawa 1998). Three hollows for the generation of parallel spot cavitation are located with a separate angle of 15 degrees. Since a hollow for the generation of isolated spot cavitation is also located on the same head, the aluminum specimen is subjected to the parallel and isolated spot cavitation simultaneously. The locations of the hollows are 76 degrees from the stagnation point (Shimizu, Tsurusaki, Hara & Nakagawa 1998).

The total gas content of the tunnel water as measured by a van Slyke's apparatus and expressed in ratio to the saturated gas content is in the range from 107 to 112 percent.

The cavitation number σ is defied as follows:

$$\sigma = (p_\infty - p_V) / (\rho v^2 / 2) \quad (1)$$

where $p_\infty$ , $p_V$, $v$, and ρ are static pressure in the working section measured at 220 mm upstream position from the hemispherical head, vapor pressure at the bulk liquid temperature, fluid velocity at the working section, and water density, respectively. Observations and erosion tests are conducted at the cavitation number of 0.91 and the flow speed ranging from 25 to 50 m/s. The duration of the erosion test is selected to be 120, 60, 12, and 7 s, for the flow speed of 25, 30, 40, and 50 m/s, respectively.

In order to investigate the structure of spot cavitation, instantaneous photographs are taken with an exposure time of approximately 1.5 μs by using a stroboscope.

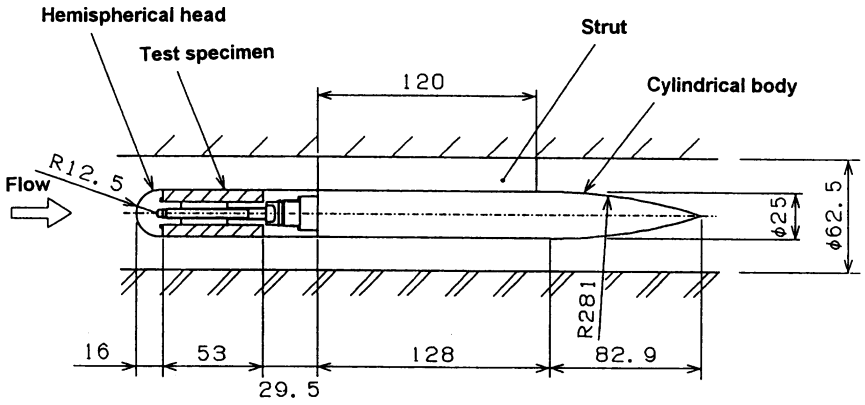


Figure 1 Hemispherical body in the test section

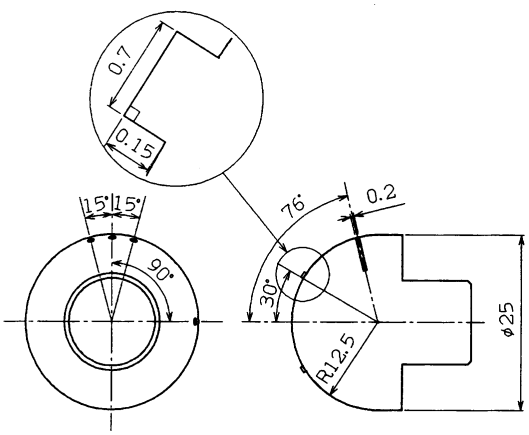


Figure 2 Hemispherical head

## 3 Experimental results and discussion

Figures 3 and 4 show examples of instantaneous photographs of the artificially generated isolated spot cavitation and parallel cavitation at $\sigma = 0.91$ and $v = 30$ m/s. The photographs are taken obliquely illuminating from above. When spot cavitation is isolated, a wedge-shaped cavity originates from the hollow downstream of the trip. Periodic release of an inverse U-shaped vortex cavity is observed in the closure region of the wedge-shaped cavity (Shimizu, Tsurusaki, Hara & Nakagawa 1998). In the case of the parallel cavitation, three wedge-shaped cavities originate from the hollows. The length and width of each wedge-shaped cavity change periodically and simultaneously. The rear parts of the wedge-shaped cavities overlap for the most part of time. However, the cavities separate each other when the length and width of each cavity become minimum. Interactions of the cavities exert influence on the release of vortex cavitation in the closure region of the main cavities. A large inverse U-shaped vortex cavity can be occasionally observed downstream of the central wedge-shaped cavity as shown in Figure 4. Figure 5 shows another examples of the photographs at $\sigma = 0.91$ and $v = 30$ m/s. The photographs are taken from above. Each wedge-shaped cavity sometimes releases a U-shaped vortex cavity independently as shown in Figure 5(a). A vortex cavity connecting the central and the lower wedge-shaped cavities can be observed in Figure 5(b).

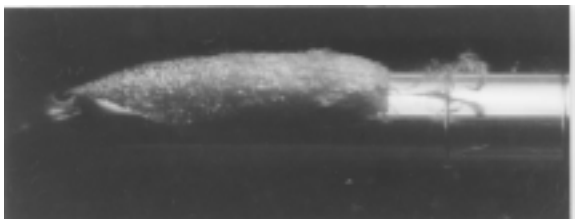

Figure 3 Isolated spot cavitation

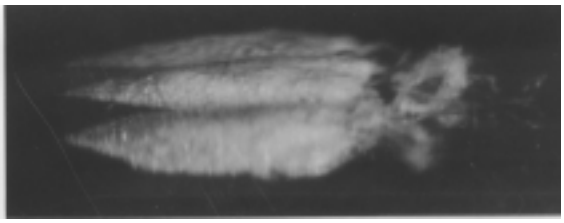

Figure 4 Parallel spot cavitation

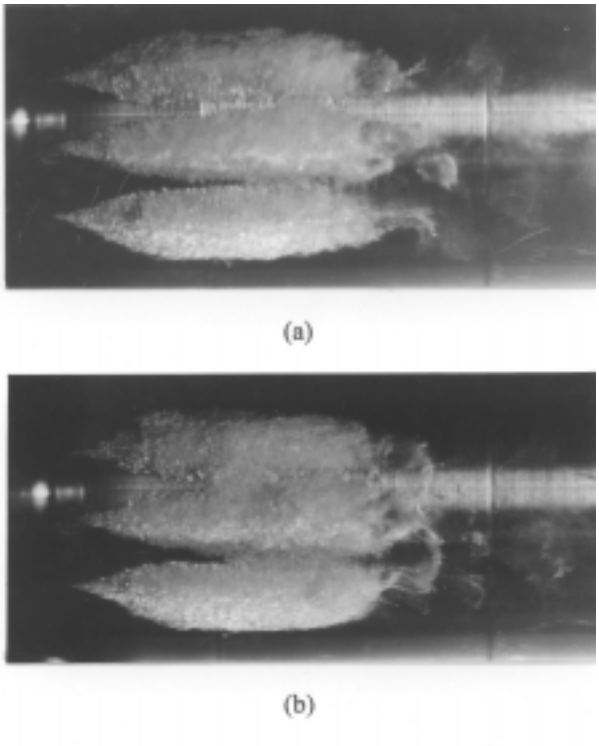


Figure 5 Release of vortex cavity in the closure region of parallel spot cavitation

Figure 6 shows the effects of the flow speed on the locations of the trailing edge of the main cavities for the cases of the isolated and the parallel spot cavitation. The trailing edge location $X$ is defined as the axial distance measured from the stagnation point of the hemispherical head. The mean trailing edge locations of the wedge-shaped cavities are the averaged values measured from the frames of VTR taken under stroboscope illumination. The cavity length of the parallel spot cavitation is slightly longer than that of the isolated cavitation. The trailing edge locations of the wedge-shaped cavities for the both cases tend to shift upstream slightly with the increase of the flow speed. The error bar represents three times of the standard deviations in the measured values. The standard deviations of the measured cavity locations are shown in Table 2. When three spot cavities occur in parallel, the cavities are rather stable. A change of the cavity length of the parallel spot cavitation is much smaller than that of the isolated spot cavitation.

The frequency of damaging blows in the range of the flow speed of 25 to 50 m/s is obtained by counting the number of damage pits on the aluminum specimen. The distributions of the pitting rate by the isolated spot cavitation and the parallel spot cavitation at $\sigma = 0.91$ and $v = 30$ m/s are shown in Figures 7 and 8, respectively. When the flow velocity $v$ is 50 m/s, the distributions of the pitting rate are shown in Figures 9 and 10. The maximum rate of pitting occurs at the downstream end or slightly upstream of the downstream end of the main cavity (Shimizu, Tsurusaki, Hara & Nakagawa 1998). In the case of the isolated spot cavitation, the pitting rate has peaks at two locations in the direction of the circumference, which suggests that the damage by the isolated spot cavitation is closely related to the release of inverse U-shaped vortex cavities. In the case of the parallel spot cavitation, however, each wedge-shaped cavity on both sides does not have two peaks of the pitting rate but has only one peak. The interaction of the wedge-shaped cavities on the release of vortex cavitation in the closure region, as shown in Figs. 4 and 5, affects the distribution of the pitting rate. When the flow speed is relatively low ($v = 30$ m/s), the pitting rate has the maximum at the downstream end of the central main cavity. With the increase of the flow speed, the pitting rates in both sides become larger than the central pitting rate.

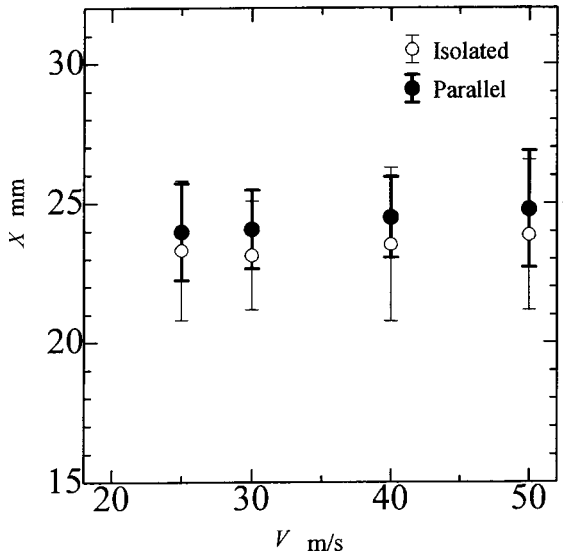


Figure 6 Trailing edge locations of main cavities

Table 2 Standard deviation of the trailing edge location

| | 25 m/s | 30 m/s | 40 m/s | 50 m/s |
|---|---|---|---|---|
| Isolated | 0.83 mm | 0.65 | 0.92 | 0.90 |
| Parallel | 0.56 | 0.47 | 0.48 | 0.70 |

The variations of the pitting rate at the maximum damage zone *Nmax* with the flow speed are compared for cases of the isolated and parallel spot cavitation as shown in Figures 11 and 12. The pits were classified roughly according to diameter as follows: below 10 μm, 10 to 20 μm, 20 to 30 μm, and above 30 μm. The total pitting rates of the isolated and parallel spot cavitation vary roughly 5th power of the flow speed. However, *Nmax* by the isolated spot cavitation is much larger than that by the parallel spot cavitation as shown in Figures 7 to 10. The exponent is smaller than that by the sheet cavitation (in the case of the sheet cavitation around the hemispherical cylindrical body, the exponent is 7.2 (Murai et al. 1997)) but the pitting rate by the spot cavitation is much larger than that by the sheet cavitation in the range of the flow speed of 25 to 50 m/s.

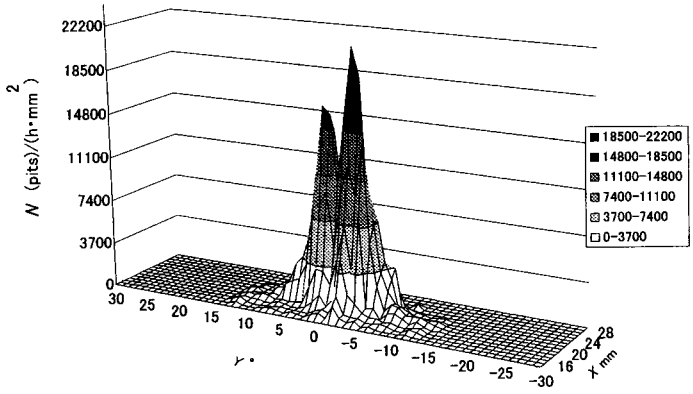


Figure 7 Pitting rate distribution by isolated spot cavitation at $v$ = 30 m/s

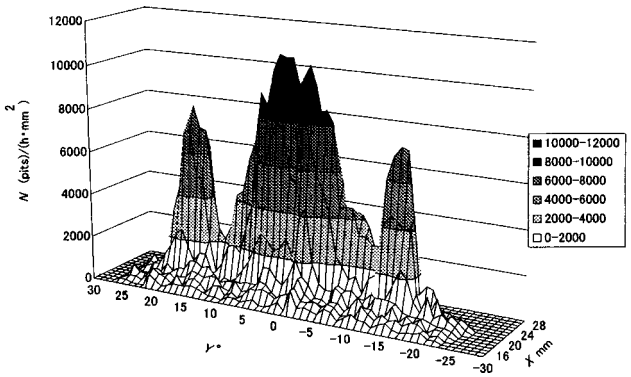


Figure 8 Pitting rate distribution by parallel spot cavitation at $v$ = 30 m/s

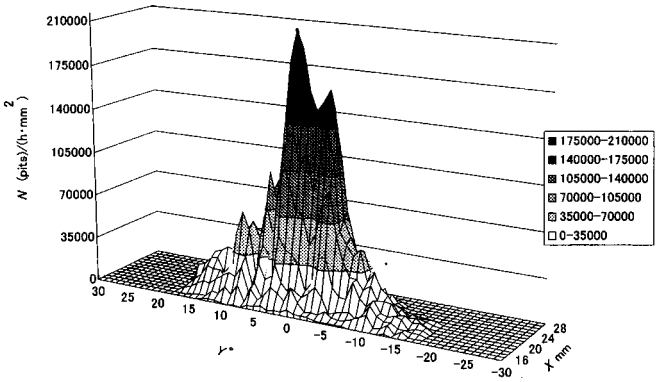


Figure 9 Pitting rate distribution by isolated spot cavitation at $v$ = 50 m/s

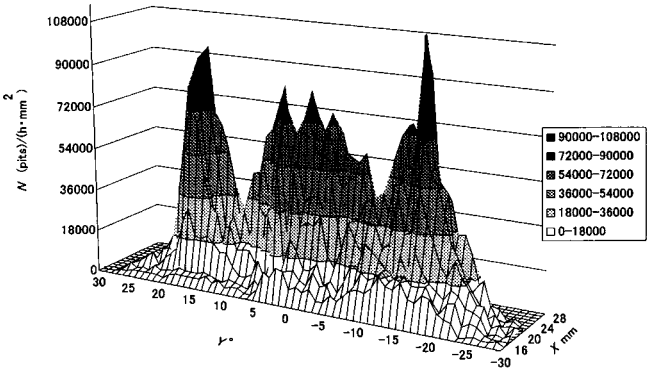


Figure 10 Pitting rate distribution by parallel spot cavitation at $v$ = 50 m/s

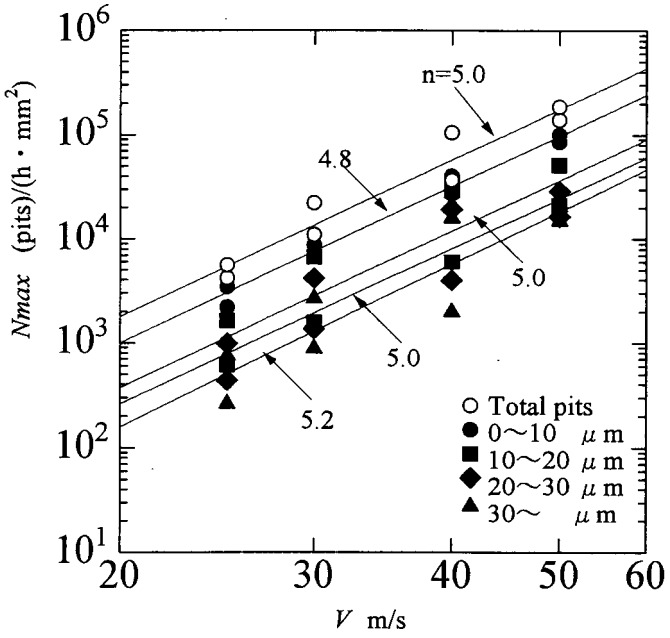


Figure 11 Variation of *Nmax* with flow speed (Isolated spot cavitation)

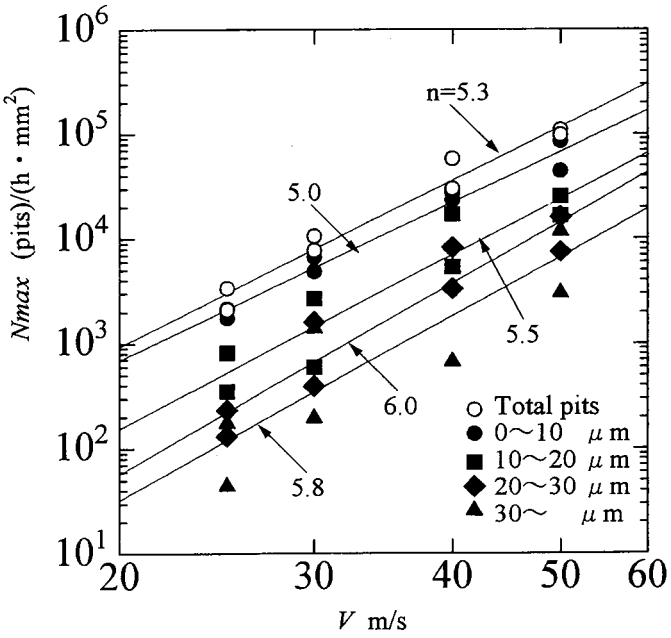


Figure 12 Variation of *Nmax* with flow speed (Parallel spot cavitation)

# 4 Concluding remarks

Experimental studies are conducted to clarify the damage due to isolated and parallel spot cavitation on a hemispherical cylindrical body. The behavior of artificially generated parallel spot cavitation is observed by using instantaneous photographs. The frequencies of damaging blows in the range of the flow speed of 25 to 50 m/s are obtained by counting the number of damaged pits on an aluminum specimen. The main conclusions are as follows:

(1) When spot cavitation occurs adjacently, the cavities become rather stable. The change of the cavity length of the parallel spot cavitation is smaller than that of the isolated spot cavitation.
(2) The pitting rate at the maximum damage zone by the parallel spot cavitation is much smaller than that by the isolated spot cavitation.
(3) The total pitting rats at the maximum damage zone by the isolated and parallel spot cavitation vary roughly 5th power of the flow speed for the both cases.

# References

Hall, J. W. and Carroll, J. A., Observations of the various types of limited cavitation on axisymmetric bodies, Trans. ASME, J. Fluids Engng, Vol. 103, 1981, pp.415-424

Huang, T. T., The effects of turbulence stimulators on cavitation inception of axisymmetric headforms, Trans. ASME, J. Fluids Engng., Vol. 108, 1986, pp.261-268

Murai, H., Nishi, S., Shimizu, S., Murakami, Y., Hara, Y., Kuroda, T., and Yaguchi, S., Velocity dependence of cavitation damage (Sheet-type cavitation), Trans. JSME, Ser. B, Vol. 63, No. 607, 1997, pp.750-756, in Japanese

Pan, S. S., Yang, Z. M., and Hsu, P. S., Cavitation inception tests on axisymmetric headhorms, Trans ASME, J. Fluids Engng., Vol. 103, 1981, pp.268-272

Shimizu, S., Tsurusaki, K., Hara, M., and Nakagawa, T., Damage due to spot cavitation on hemispherical cylindrical body, Proc. 3rd International Symposium on Cavitation, Grenoble France, 1998, Vol. 2, pp.163-169